NAD^+ Redox Imbalance in the Heart Exacerbates Diabetic Cardiomyopathy

Ying Ann Chiao, PhD[1], Akash Deep Chakraborty, PhD[1,2], Christine M. Light, BS[2], Rong Tian, MD PhD[3], Junichi Sadoshima, MD PhD[4], Xiaojian Shi, PhD[5], Haiwei Gu PhD[5], Chi Fung Lee PhD[2,6*]

[1]Aging and Metabolism Research Program, [2]Cardiovascular Biology Research Program, Oklahoma Medical Research Foundation, Oklahoma City, OK

[3]Mitochondria and Metabolism Center, University of Washington, Seattle, WA

[4]Department of Cell Biology and Molecular Medicine, Rutgers New Jersey Medical School, Newark, NJ

[5]Arizona Metabolomics Laboratory, College of Health Solutions, Arizona State University, Scottsdale, AZ

[6]Department of Physiology, University of Oklahoma Health Sciences Center, Oklahoma City, OK

*** Address correspondence to:**

Chi Fung Lee, PhD
Cardiovascular Biology Research Program, MS 45
Oklahoma Medical Research Foundation
825 NE 13th Street
Oklahoma City, OK 73104, USA
Tel: 405-271-1703
Fax: (405) 271-7417
chifung-lee@omrf.org

Short title: NAD^+ redox balance and diabetic cardiomyopathy

Word count: 4000

Number of tables and figures: 6

Abstract

Background: Diabetes is a risk factor of heart failure, and chronic diabetic stress leads to cardiac dysfunction. Diabetic tissues are associated with NAD^+ redox imbalance; however, the hypothesis that NAD^+ redox imbalance leads to dysfunction of diabetic hearts has not been tested. In this study, we employed mouse models with altered NAD^+ redox balance to test the hypothesis and to characterize the underlying mechanism.

Methods and Results: Type 1 diabetes was induced in C57/BL6 mice by streptozotocin injections, and diabetic cardiomyopathy (DCM) was allowed to develop for 16-weeks. Chronic diabetic stress led to cardiac dysfunction and lowered NAD^+/NADH ratio. The same diabetogenic regimen was administered to cardiac-specific Ndufs4-KO mice (cKO), a model of lowered cardiac NAD^+/NADH ratio without overt baseline dysfunction. Cardiac NAD^+ redox imbalance in cKO hearts exacerbated systolic and diastolic dysfunction of diabetic mice in both sexes. Collagen levels and transcript analyses of fibrosis and extracellular matrix-dependent pathways showed no change in diabetic cKO hearts, suggesting that the exacerbated cardiac dysfunction was likely due to cardiomyocyte dysfunction. We found that cardiac NAD^+ redox imbalance promoted SOD2 acetylation and protein oxidation, and regulated TnI phosphorylation in diabetic cKO hearts. Elevation of cardiac NAD^+ levels by NAMPT over-expression mitigated NAD^+ redox imbalance in diabetic cKO mice, reversed SOD2 acetylation and TnI phosphorylation, and alleviated cardiac dysfunction.

Conclusion: Our results show that NAD^+ redox imbalance to regulate protein acetylation and phosphorylation is a critical mediator of the progression of DCM, and suggest the therapeutic potential of harnessing NAD^+ metabolism in DCM.

Introduction

Diabetes is characterized as a loss of glycemic control, and is a major risk factor of heart failure. Epidemiological studies show a positive correlation of hyperglycemia with the increased risk of heart failure in both Type 1 and Type 2 diabetes patients [1-3]. Diabetic cardiomyopathy (DCM) is defined as diabetes-associated cardiac dysfunction independent of coronary artery diseases or other confounding cardiovascular diseases [4]. Mechanisms such as mitochondrial dysfunction and oxidative stress have been identified [5]. However, how altered metabolism in diabetes, in particular NAD^+-dependent pathways, leads to cardiac dysfunction is not fully understood.

NAD^+-dependent pathways have emerged to play critical roles in metabolism-driven disease progression [6]. NAD^+ mediates electron transfer and redox reactions in metabolism [7]. The oxidized form of NAD^+ (NAD^+) is converted to the reduced form (NADH) to mediate substrate catabolism (e.g. glycolysis) via many oxidoreductase-dependent metabolic enzymes. The recycling of NADH to NAD^+, and NAD^+ redox balance (high NAD^+/NADH ratio) are essential to maintain substrate catabolism and ATP synthesis. The functions of NAD^+ have been vastly expanded with the discovery of NAD^+-consuming enzymes, e.g. Sirtuins, NAD^+-dependent deacetylases. Sirtuins remove acyl modifications on lysine residues of proteins by turning NAD^+ into nicotinamide (NAM) and acyl-ADPR. Activation of Sirtuins is generally cytoprotective and inhibition of Sirtuins promotes pathogenesis in many metabolic diseases [8-11]. The availability of NAD^+ to Sirtuins, via changes in the NAD^+/NADH ratio or the NAD^+ pool, is crucial to regulate mitochondrial and cellular functions. To replenish the loss of NAD^+ consumed by Sirtuins, NAD^+ is synthesized by several biosynthetic pathways. The NAD^+ salvage pathway is the

dominant pathway used in a mouse heart [12]: NAM generated from the reactions of Sirtuins is recycled to synthesize nicotinamide mononucleotide (NMN) by nicotinamide phosphoribosyltransferase (NAMPT), the rate-limiting enzyme of the salvage pathway. NMN is then converted into NAD^+ by nicotinamide mononucleotide adenylyltransferases (NMNATs). Elevating NAD^+ levels by activation of the NAD^+ biosynthetic pathways is therapeutic to diseases [13-20]. We previously showed that NAD^+-dependent acetylation contributes to pressure overload-induced heart failure, and elevation of NAD^+ levels alleviates the cardiac dysfunction [21, 22]. Hyperglycemia is associated with decreased NAD^+/NADH ratio, and promotes protein hyperacetylation and mitochondrial dysfunction in diabetic organs [16, 23-27]. Although these data support a hypothesis that NAD^+ redox imbalance in diabetic hearts promotes cardiac dysfunction, this hypothesis has not been directly tested.

We previously generated a mouse model of mitochondrial dysfunction by deleting Ndufs4, a complex I protein, only in the hearts (cardiac Ndufs4-KO, cKO) [21]. Complex I deficiency in cKO mice leads to lowered cardiac NAD^+/NADH ratio, but surprisingly these mice have normal cardiac function [21, 22]. In this study, we challenged this mouse model of latent cardiac NAD^+ redox imbalance with diabetic stress, and examined the progression of DCM. We found that cKO mice showed exacerbated cardiac dysfunction in response to diabetic stress, while elevation of cardiac NAD^+ levels with cardiac-specific NAMPT transgenic mice (NAMPT) [28] ameliorated the decline. The exacerbated cardiac dysfunction was associated with increased global protein and SOD2 acetylation, oxidative stress and myofilament protein phosphorylation, but not enhanced fibrosis.

Research Design and Methods

Animals care and experiments

All animal care and procedures were approved by the Institutional Animal Care and Use Committee (IACUC) at the Oklahoma Medical Research Foundation and the University of Washington. All procedures were performed in accordance with IACUC regulations. Cardiac-specific Ndufs4 (cKO) mice were generated from the breeding of Ndufs4$^{flox/flox}$ mice with alpha-MHC-Cre expressing mice [21]. Expression of NAMPT in the heart was achieved by crossing a cardiac-specific NAMPT mouse line with cKO mice [21, 28]. Three to four-month-old mice were used at the beginning of this study. Streptozotocin (STZ) was used to induce beta-cell and insulin depletion. STZ in citrate buffer was given to mice intraperitoneally at 50 mg/kg for five days in chronic diabetic experiments, and once in acute STZ experiment. Body weights were measured before, 8 weeks or 15 weeks after STZ injection in different experiments.

Systolic function and geometry were assessed by echocardiography with parasternal long axis and M-mode images using VEVO 2100 system (VisualSonics) on lightly-anesthetized mice. Parameters such as fractional shortening (FS), and left ventricular internal diameter at diastole (LVID;d) were measured and calculated by using the software package in the VEVO 2100 system when the heart rate was within 500-600 beats per minute. Using the same system, parameters describing diastolic function were measured: E'/A' ratio was measured by tissue doppler imaging of mitral annulus. The e peaks were measured by images from transmitral pulse-wave doppler, and e/E' ratio was also calculated. Myocardial performance index (MPI) was calculated as the sum of isovolumetric contraction time (IVCT) and isovolumetric relaxation time (IVRT) divided by

ejection time (ET). These parameters were measured and calculated by averaging three cardiac cycles.

Tissue harvest and processing

On the day of tissue harvest, mice were subjected to fasting for 6 hours and anesthetized using pentobarbital. Rib cages were cut open to expose hearts for blood collection by cardiac puncture. Heart weight, wet and dry lung weights, and tibia length were measured post-mortem. Cardiac tissue samples were collected and snap-frozen with liquid nitrogen. Frozen tissues were pulverized using a Tissuelyzer II (Qiagen) for biochemical assays.

NAD^+ assay

10-15 mg of pulverized cardiac tissue were used for measurement of NAD^+ and NADH levels using commercially available kits (BioAssay) under the manufacturer's instructions.

Analysis of mRNA levels

Total RNA was extracted from pulverized cardiac tissues using RNeasy fibrous tissue mini kit (Qiagen). RNA amount was quantified by nanodrop. 0.5 ug of RNA was used for cDNA synthesis using Maxima first stand kit (ThermoFisher). All cDNA products were diluted by ten times with water. Diluted cDNAs were subjected to quantitative PCR reaction using Sybr green probes and primers from extracellular matrix and adhesion molecules genes (RT2 Profiler PCR Array). Real time PCR reaction was performed with CFX96 thermocycler (Biorad).

Western blotting

Pulverized cardiac tissues were homogenized in RIPA buffer (Sigma) with protease and phosphatase inhibitor cocktail (Halt, ThermoFisher) and deacetylase inhibitors (10 mM nicotinamide, 10 uM Trichostatin A). Protein concentrations of samples were determined by BCA assay (ThermoFisher), and equal amounts of protein (20 ug per sample) were loaded for SDS-PAGE using the Criterion system. Proteins were transferred onto PVDF membrane using Criterion Blotter (Biorad). Blots were blocked in 5% BSA-TBST. Primary antibodies were diluted using 5% BSA-TBST. Antibodies from the following companies were used for Western blot analysis: acetyl-lysine (1:1000, 9441-Cell signaling), SDHA (1:10000, ab14715-Abcam), SOD2 (1:3000, PA5-30604-Thermo Fisher) SOD2-K68Ac (1:10000, ab137037-Abcam), TnI-S150Pi (1:1000, PAS-35410-Thermo), TnI-S23/24Pi (1:1000, 4004S-Cell Signaling), TnI (1:1000, 4002S-Cell Signaling), MyBPC-S282Pi (1:2000, ALX-215-057-R050) and MyBPC (1:1000, SC-137237, Santa Cruz). Antibodies were diluted in 5% BSA-TBST. Protein bands were visualized with chemiluminescence assay (Pierce) with secondary antibodies coupled with HRP using the G-Box imaging system. The protein abundance was analyzed by densitometry with ImageJ.

Plasma analyses

Mouse blood was collected using cardiac puncture during tissue harvest. Blood samples were incubated in EDTA collection tube (BD Diagnostics). After thorough mixing, blood samples were centrifuged at 300 g for five minutes at room temperature. Plasma samples were collected as supernatant and snap-frozen by liquid nitrogen. Glucose levels in plasma were measured by test strips (AlphaTRAK 2 blood glucose tests). Plasma insulin levels were measured by a commercially available kit (Crystalchem).

In metabolite analysis, acetonitrile (ACN), methanol (MeOH), ammonium acetate, and acetic acid, all LC-MS grade, were obtained from Fisher. Ammonium hydroxide was bought from Sigma-Aldrich. PBS was bought from GE Healthcare. The standard compounds were purchased from Sigma-Aldrich and Fisher.

Frozen plasma samples were thawed overnight under 4°C. 500 μL of MeOH and 50 μL of internal standard solution were added ti each sample (50 μL) for protein precipitation and metabolite extraction (containing 1,810.5 μM $^{13}C_3$-lactate and 142 μM $^{13}C_5$-glutamic acid). The mixture was vortexed and stored at -20°C, followed by centrifugation at 14,000 RPM. The supernatants were collected and dried using a CentriVap Concentrator (Labconco). The dried samples were reconstituted with 40% PBS/60% ACN. A pooled sample was used as the quality-control (QC) sample.

The targeted LC-MS/MS method was used in a growing number of studies [29-31]. Briefly, all LC-MS/MS experiments were performed on an Agilent 1290 UPLC-6490 QQQ-MS system. Each sample was injected twice for analysis using negative and positive ionization mode. Both chromatographic separations were performed in hydrophilic interaction chromatography (HILIC) mode on a Waters XBridge BEH Amide column (Waters). The mobile phase was composed of Solvents A (10 mM ammonium acetate, 10 mM ammonium hydroxide in 95% H_2O/5% ACN) and B (10 mM ammonium acetate, 10 mM ammonium hydroxide in 95% ACN/5% H_2O). After the initial 1 min isocratic elution of 90% B, the percentage of Solvent B decreased to 40% at t=11 min. The composition of Solvent B maintained at 40% for 4 min (t=15 min), and then the percentage of B gradually went back to 90%, to prepare for the next injection.

The mass spectrometer is equipped with an electrospray ionization (ESI) source. Targeted data acquisition was performed in multiple-reaction-monitoring (MRM) mode. TThe extracted MRM peaks were integrated using Agilent MassHunter Quantitative Data Analysis.

Histology

One-millimeter thick heart tissues were cut cross-sectionally at the mid-section and fixed with 4% paraformaldehyde for 24 hours. The tissues were changed to 70% ethanol and fixed tissues were processed for paraffin embedding and sectioning. Tissue sections were stained with trichrome for collagen analysis. The trichrome stained slides were scanned with an Aperio Scanscope AT2 (Leica) at 40x. Quantitative image analysis of whole stained sections was performed using Aperio Brightfield Image Analysis Toolbox software and a color deconvolution algorithm was used to measure RGB color vectors of blue (positive trichrome stain) and total stained tissue area. The quantitative analysis of cardiac fibrosis for the percentages of collagen (trichrome-blue stain component) and total stained tissue area (mm^2) was performed.

Statistical analysis

For comparisons involving two groups, unpaired 2-tailed t-tests were used. All analyses were performed using GraphPad Prism 7.0. All data are expressed as mean ± SEM, and a $p<0.05$ was considered significant. Metabolite levels were statistically analyzed by MetaboAnalyst 4.0. Adjusted P-value (FDR) cutoff for the dataset was set at 0.05. Raw data are available as supplementary materials. Heatmaps were generated by Morpheus.

Results

16 weeks of diabetic stress lowered cardiac function and NAD^+/NADH ratio

We induced diabetes using streptozotocin (STZ), a drug that promotes beta-cell death and leads to loss of glycemic control. STZ treatment to C57/BL6 wildtype mice led to significant increase in fasting blood glucose levels 16 weeks after treatment (Figure 1A). 16 weeks of diabetic stress in wildtype mice led to decline in contractile and relaxation function of the heart: Contractile function represented by fractional shortening (FS) decreased in STZ-treated diabetic mice (Figure 1B). E'/A' ratio decreased, and e/E' ratio and isovolumic relaxation time (IVRT) increased in diabetic mice, indicating relaxation dysfunction (Figure 1C-F). Decline in cardiac function was associated with a lowered NAD^+/NADH ratio (Figure 1G). The damage of STZ is not specific to beta cells and impairments on function of cardiomyocytes were reported [32]. STZ may also lower NAD^+ levels by PARP activation [33]. Therefore, we examined the acute effects of STZ treatment on the heart. We observed that acute STZ treatment (1 day) did not affect cardiac function, NAD^+ pool size, and fasting glucose levels (Supp. Figure 1A-D). Since STZ is rapidly metabolized and excreted by rodents [34], the lowered NAD^+/NADH ratio of hearts 16 weeks after STZ treatment was due to the chronic diabetic stress (Figure 1A) similarly observed in other diabetic tissues [16, 23-27], rather than by the direct STZ-mediated toxicity to the heart.

NAD^+ redox imbalance exacerbated dysfunction of diabetic hearts

Although NAD^+ redox imbalance is found in diabetic hearts (Figure 1G), the causal role of the lowered NAD^+/NADH ratio induced by diabetic stress to cardiac dysfunction was not directly examined in our initial studies. Therefore, we employed cardiac-specific

Ndufs4-KO mice (cKO), a mouse model with lowered cardiac NAD^+/NADH ratio and normal cardiac function [21] to determine how NAD^+ redox imbalance changes the progression of DCM. Male control and cKO mice were subjected to 8-week, STZ-induced diabetic stress (Figure 2A). STZ treatment led to insulin depletion, and the extent of insulin depletion was similar in control and cKO mice (Supp. Figure 2A). Fasting blood glucose levels of control and cKO mice 8-week after STZ treatment were up-regulated and similar (Supp. Figure 2B). We next analyzed plasma samples collected from diabetic control and diabetic cKO mice by quantitative metabolomics. Of 159 aqueous and 85 lipid metabolites surveyed, no significant change in levels was observed (Supp. Figure 2C-D, FDR cutoff < 0.05, raw data available in supplementary table). The plasma metabolomic analyses suggested that control and cKO hearts experienced similar diabetic stress. Despite the similar extent of diabetic stress, diabetic cKO mice exhibited reduced cardiac NAD^+/NADH ratio compared to diabetic control mice (Figure 2B, Supp Figure 2). The diabetic stress promoted a decline in contractile function of control mice, which was exacerbated in cKO mice 2, 4, and 8 weeks after initiation of diabetic stress (Figure 2C, Supp Figure 3). The exacerbated diastolic dysfunction in diabetic cKO mice was also observed by a lowered E'/A' ratio, an increased e/E' ratio and IVRT, and an elevated myocardial performance index, MPI (Figure 2D-G). Left ventricular dilation, cardiac hypertrophy and lung edema did not change in diabetic cKO hearts (Figure 2H-J).

We performed the same diabetogenic protocol (Figure 2A) in female control and cKO mice. Similarly, diabetic stress promoted contractile and relaxation dysfunction in diabetic control mice, which was significantly worsened in diabetic cKO mice (Figure 3A-C, Supp Figure 3). MPI, left ventricular dilation, cardiac hypertrophy, and lung edema

were unchanged (Figure 3D-G). The results suggest that NAD^+ redox imbalance is a positive regulator for the progression of DCM in both sexes.

Tissue fibrosis was not associated with exacerbated DCM induced by NAD^+ redox imbalance

Diabetic hearts are often associated with increased fibrosis, and cardiac dysfunction, especially relaxation dysfunction, is dependent on tissue fibrosis [35]. We therefore quantified tissue collagen contents of mid-sectioned heart slices by trichrome staining. We observed similar fibrosis levels (~4%) in diabetic control and diabetic cKO hearts (Figure 4A). Consistent to this histological observation, expression of extracellular matrix (ECM)-related genes showed no change between diabetic control and diabetic cKO hearts: transcript levels of Adamts proteinases, integrins, laminins, matrix metalloproteinases and collagen subtypes (Figure 4B-C, Supp Figure 4A-C) were not different. These results suggest that altered ECM environment and fibrosis do not account for the exacerbated dysfunction, but cardiomyocyte dysfunction may be the culprit.

Elevated SOD2 acetylation promoted oxidative modification in diabetic cKO hearts

NAD^+ is required for deacetylation by Sirtuins, and NAD^+ redox imbalance has been associated with protein hyperacetylation. Therefore, we explored the roles of NAD^+ redox imbalance in regulating protein acetylation in diabetic hearts. NAD^+ redox imbalance elevated global protein acetylation in diabetic cKO hearts (Figure 5A, Supp. Figure 4D). Specifically, we observed that acetylation levels of superoxide dismutase 2 at lysine-68 (SOD2-K68Ac) were elevated in diabetic cKO hearts (Figure 5B, Supp. Figure 4E). SOD2-K68Ac is known to suppress its antioxidant activity [36], suggesting that

diabetic cKO hearts could be more prone to oxidative stress. Consistently, levels of protein carbonylation, an irreversible protein oxidative modification used as a marker of oxidative stress, were elevated in diabetic cKO hearts (Figure 5C, Supp. Figure 4F). Transcript levels of NADPH oxidase (Nox) isoforms, key ROS generating proteins, were similar in diabetic control and diabetic cKO hearts (Figure 5D). These results support the role of NAD^+ redox imbalance in regulating oxidative stress by promoting SOD2 acetylation in DCM.

NAD^+ redox imbalance regulated TnI phosphorylation

We then examined if phosphorylation of myofilament proteins, which control cardiac contraction and relaxation, were altered by NAD^+ redox imbalance in diabetic hearts. Phosphorylation states of troponin I (TnI) and myosin binding protein c (MyBPc) can modulate contractile and relaxation properties of the myocardium in diseased hearts [37, 38]. TnI is an inhibitory subunit of troponin, and phosphorylation of TnI at S150 and at S23/24 (TnI-S150Pi and TnI-S23/24Pi) has been shown to coordinately regulate myofilament calcium sensitivity as an adaptive response in ischemic hearts [39, 40]. Diabetic cKO hearts displayed increased levels of TnI-S150Pi compared to diabetic control, while levels of TnI-S23/24Pi remained unchanged (Figure 5E-F, Supp Figure 4G-H). As TnI-S150Pi prolongs calcium dissociation [39], these results suggest that NAD^+ redox imbalance induces TnI-S150 phosphorylation to exacerbate diastolic dysfunction (Figure 2D-E) and increase IVRT (Figure 2F) in DCM. MyBPc is a sarcomeric protein that interacts with myosin and actin, and phosphorylation of MyBPc fine-tunes actin-myosin cross-bridge cycling to regulate cardiac contraction-relaxation. MyBPc S282 phosphorylation (MyBPc-S282Pi) is critical for normal cardiac function and reduced

MyBPc-S282Pi has been observed in failing hearts [38]. Levels of MyBPc-S282Pi were unchanged in diabetic cKO hearts, suggesting that it is not responsible for the worsened cardiac function.

Elevation of NAD^+ levels ameliorated dysfunction of diabetic cKO hearts

To validate the causal role of NAD^+ redox imbalance in DCM, we examined the effects of elevation of cardiac NAD^+ levels on DCM development in diabetic cKO mice. Transgenic mice expressing NAMPT in the heart (NAMPT) were crossed with cKO mice [22]. The same experimental protocol was used on cKO and cKO:NAMPT mice (Figure 2A, 6A). Expression of NAMPT in the heart increased NAD^+/NADH ratio and NAD^+ pool in diabetic cKO hearts, and improved systolic and diastolic dysfunction (Figure 6B-F, Supp Figure 5A). These improvements occurred despite the similar extents of hyperglycemia in cKO and cKO:NAMPT mice (Supp. Figure 5B). The body weight changes 8 weeks after diabetes induction were similar (Supp. Figure 5C). Heart rate, left ventricular dilation, hypertrophy, and lung edema were also unchanged (Supp Figure 5D-G). Importantly, NAMPT expression lowered the levels of SOD2-K68Ac and TnI-S150Pi in diabetic cKO hearts, while TnI-S23/24Pi levels were similar (Figure 6G-I, Supp. Figure 4I-K). These results further establish the causal roles of NAD^+ redox imbalance, and its regulations on protein acetylation and phosphorylation, in the progression of DCM.

Discussion

Diabetes increases the risk of heart failure and causes diabetic cardiomyopathy (DCM). Although mechanisms such as lipotoxicity, oxidative stress and mitochondrial dysfunction are proposed [5], the mechanisms by which metabolic stresses in diabetes lead to cardiac dysfunction are not fully understood. Hyperglycemia and dyslipidemia are the hallmarks of diabetes, and diabetes alters cardiac metabolism such as substrate utilization [5]. NAD^+ is an important redox cofactor for glucose and lipid oxidation. Changes in NAD^+ metabolism such as NAD^+ redox imbalance emerge as critical mediators of disease pathogeneses such as heart failure [21, 22]. NAD^+ redox imbalance has long been observed in tissues from diabetic mice [16, 23-25], supporting a hypothesis that diabetes-driven NAD^+ redox imbalance promotes DCM. In this study, we demonstrated the causal role of NAD^+ redox imbalance in promoting DCM. The key findings in supporting this notion are that 1) NAD^+/NADH ratio decrease in hearts after chronic diabetes; 2) a pre-existing, lowered cardiac NAD^+/NADH ratio exacerbates the progression of DCM, which is alleviated by elevating NAD^+ levels; and 3) NAD^+ redox imbalance mediates dysfunction of diabetic hearts in part by increased oxidative stress and regulation of myofilament protein phosphorylation, but not by enhanced cardiac fibrosis.

Diabetic stress is associated with lowered NAD^+/NADH ratio, aka pseudohypoxia, in tissues such as hearts [24, 41]. Functional decline in diabetic hearts has also been reported in parallel [5]. However, whether NAD^+ redox imbalance causes DCM has not been directly tested. We found that 16-week diabetic stress lowered cardiac NAD^+/NADH ratio, accompanied by systolic and diastolic dysfunction. Importantly, we observed that the cardiac-specific mouse model with lowered NAD^+/NADH ratio exhibits exacerbated

DCM, which can be rescued by restoration of NAD^+/NADH ratio in the heart (Figure 2,3,6). This is the first direct evidence to establish the causal role of NAD^+ redox imbalance in the progression of DCM. A recent report showed the role of hepatic NAD^+ reductive stress (low NAD^+/NADH ratio) in determining changes in diabetes-induced metabolite levels (alpha-hydroxybutyrate) and insulin resistance in vivo [42], supporting the pathogenic role of NAD^+ redox imbalance in diabetes and its complications. We previously demonstrated that NAD^+ redox imbalance is a critical mediator in pressure overload-induced heart failure [22]. Whether diabetes and hypertension have additive or synergistic effects on cardiac NAD^+ redox imbalance to promote cardiac dysfunction remain to be determined.

While the causal role of NAD^+ redox imbalance for DCM is well-supported by our current data, the origin of NAD^+ redox imbalance induced by diabetic stress is still obscure. Evidence linking hyperglycemia and dyslipidemia in promoting NAD^+ redox imbalance was reported [27, 43]. Mitochondrial dysfunction and impaired NADH redox shuttles such as NAD^+-dependent malate aspartate shuttle (MAS) are important mediators of the lowered NAD^+/NADH ratio [27, 44, 45]. MAS delivers cytosolic NADH to electron transport chain for ATP generation. Interestingly, MAS activity is suppressed in hypertrophied hearts in a NAD^+ redox balance-dependent manner [22, 46, 47]. Decreased activities of MAS and mitochondria as an electron sink in diabetic hearts may lead to NAD^+ redox imbalance. However, detailed mechanisms how hyperglycemia and dyslipidemia promote impairments of NADH redox shuttles and dysfunction of diabetic hearts remains to be established.

We did not observe increased fibrosis associated with exacerbated dysfunction of diabetic cKO hearts. Fibrosis is a hallmark of heart disease of different etiologies,

especially in diabetic hearts [35], and we did observe slight increase in cardiac fibrosis from STZ-treated diabetic hearts (Supp. Figure 4J). The similar extents of fibrosis in diabetic control and diabetic cKO hearts, however, suggests that cardiomyocyte dysfunction plays an instrumental role in further impairment of cardiac function by NAD^+ redox imbalance. This can be mediated by elevated SOD2 acetylation and oxidative stress in diabetic cKO hearts. Other NAD^+-sensitive protein acetylation is likely at play for cardiac dysfunction of DCM, e.g. sensitized permeability transition pore by acetylation [22].

Our data showed that diabetic cKO hearts displayed elevated TnI-S150Pi, exacerbated diastolic dysfunction and prolonged IVRT, which are all restored by NAMPT expression. AMPK-dependent TnI-S150Pi increases myofilament calcium sensitivity and prolong calcium dissociation [37, 39, 40], while TnI-S23/24Pi decrease calcium sensitivity and accelerates calcium dissociation [37]. Combination of TnI-S150Pi and TnI-S23/24Pi retains calcium sensitivity and accelerates calcium dissociation, playing an adaptive role during ischemic injury [37]. Increased TnI-S150Pi without changes in TnI-S23/24Pi in diabetic cKO hearts and NAD^+-dependent reversal of TnI-S150Pi and diastolic function would suggest that NAD^+ redox imbalance preferentially regulate TnI-S150Pi, playing a maladaptive role for diastolic dysfunction. The mechanisms by which NAD^+ redox imbalance in diabetes regulates TnI phosphorylation are to be identified.

It is conceivable that the disease mechanisms of DCM involve other NAD^+-dependent pathways beyond NAD^+ redox imbalance and protein acetylation reported here. NAD^+ metabolism involves metabolites and enzymes in the NAD^+ consumption, synthesis and redox pathways, coordinating cellular NAD^+ homeostasis [48]. Our study employed cardiac-specific perturbations of NAD^+ redox balance (cKO and NAMPT) and

supported the roles of cardiac NAD^+ redox imbalance in DCM. However, we cannot rule out the contributions of NAD^+ metabolites and systemic changes in NAD^+ metabolism (e.g. plasma NAD^+ metabolites and extracellular NAMPT) induced by diabetic stress in promoting cardiac dysfunction. Metabolites in the NAD^+ salvage pathway, e.g. nicotinamide mononucleotide or nicotinamide riboside, are prime agents for pharmacologic elevation of NAD^+ levels for heart disease [22, 49]. In addition, the benefit of activation of NAD^+ synthesis by harnessing the de novo pathway and the role of NMRK2 up-regulation in cardiomyopathy have been reported [49, 50]. Therefore, further assessments of changes in NAD^+ metabolism in DCM are warranted, and will likely identify new targets for therapy. A limitation of this study is that we employed a STZ-induced Type 1 diabetic model, and the results cannot be generalized to Type 2 diabetes models (e.g. high-fat diet feeding). Further studies are needed to determine how NAD^+ redox imbalance affects DCM progression in responses to Type 2 diabetes.

This study establishes the causal role of NAD^+ redox imbalance in DCM. Our results support that cardiac-specific NAD^+ redox imbalance mediates cardiac dysfunction in DCM in both sexes. This highlights the importance to identify adaptive and maladaptive mechanisms triggered by NAD^+ redox imbalance and altered NAD^+ metabolism in DCM. Our pre-clinical data also demonstrate a benefit of expanding the NAD^+ pool as therapy for DCM.

Acknowledgements

CFL designed and performed the experiments, interpreted the data, and wrote the manuscript. YAC performed experiments and wrote the manuscript. ADC, XS, HG, and CML performed the experiments and analyzed the data. CFL is the guarantor of the study and has full access to all the data in the study and takes responsibility for the integrity of the data and accuracy of the data analysis.

RT and JS kindly provided mouse models. All authors have reviewed and edited the manuscript.

Sources of Funding

This work has been supported in part by research funds from the American Heart Association, 17SDG33330003, from a recruitment grant and a pilot grant of the Presbyterian Health Foundation, and from a research grant of the Oklahoma Center for Adult Stem Cell Research (all to CFL).

This work has also been supported by the National Institute of Health, K99AG051735 and R00AG051735 (both to YAC). NW BioTrust and NWBioSpecimen, are supported by the National Cancer Institute grant P30 CA015704, Institute of Translational Health Sciences grant UL1 TR000423, the University of Washington School of Medicine and Department of Pathology.

Disclosures

No financial or non-financial competing interest is disclosed associated with the investigation in this manuscript by all authors.

References

1. Kannel WB, Hjortland M and Castelli WP. Role of diabetes in congestive heart failure: the Framingham study. *Am J Cardiol*. 1974;34:29-34.

2. Authors/Task Force M, Ryden L, Grant PJ, Anker SD, Berne C, Cosentino F, Danchin N, Deaton C, Escaned J, Hammes HP, Huikuri H, Marre M, Marx N, Mellbin L, Ostergren J, Patrono C, Seferovic P, Uva MS, Taskinen MR, Tendera M, Tuomilehto J, Valensi P, Zamorano JL, Guidelines ESCCfP, Zamorano JL, Achenbach S, Baumgartner H, Bax JJ, Bueno H, Dean V, Deaton C, Erol C, Fagard R, Ferrari R, Hasdai D, Hoes AW, Kirchhof P, Knuuti J, Kolh P, Lancellotti P, Linhart A, Nihoyannopoulos P, Piepoli MF, Ponikowski P, Sirnes PA, Tamargo JL, Tendera M, Torbicki A, Wijns W, Windecker S, Document R, De Backer G, Sirnes PA, Ezquerra EA, Avogaro A, Badimon L, Baranova E, Baumgartner H, Betteridge J, Ceriello A, Fagard R, Funck-Brentano C, Gulba DC, Hasdai D, Hoes AW, Kjekshus JK, Knuuti J, Kolh P, Lev E, Mueller C, Neyses L, Nilsson PM, Perk J, Ponikowski P, Reiner Z, Sattar N, Schachinger V, Scheen A, Schirmer H, Stromberg A, Sudzhaeva S, Tamargo JL, Viigimaa M, Vlachopoulos C and Xuereb RG. ESC Guidelines on diabetes, pre-diabetes, and cardiovascular diseases developed in collaboration with the EASD: the Task Force on diabetes, pre-diabetes, and cardiovascular diseases of the European Society of Cardiology (ESC) and developed in collaboration with the European Association for the Study of Diabetes (EASD). *Eur Heart J*. 2013;34:3035-87.

3. Lind M, Bounias I, Olsson M, Gudbjornsdottir S, Svensson AM and Rosengren A. Glycaemic control and incidence of heart failure in 20,985 patients with type 1 diabetes: an observational study. *Lancet*. 2011;378:140-6.

4. Boudina S and Abel ED. Diabetic cardiomyopathy, causes and effects. *Rev Endocr Metab Disord*. 2010;11:31-9.

5. Ritchie RH and Abel ED. Basic Mechanisms of Diabetic Heart Disease. *Circ Res*. 2020;126:1501-1525.

6. Imai S and Guarente L. NAD+ and sirtuins in aging and disease. *Trends Cell Biol*. 2014;24:464-71.

7. Warburg O and Christian W. Pyridin, the hydrogen-transferring component of the fermentation enzymes (pyridine nucleotide). *Biochemische Zeitschrift (in German)*. 1936;287:291.

8. He W, Newman JC, Wang MZ, Ho L and Verdin E. Mitochondrial sirtuins: regulators of protein acylation and metabolism. *Trends Endocrinol Metab*. 2012;23:467-76.

9. Guarente L. Calorie restriction and sirtuins revisited. *Genes Dev*. 2013;27:2072-85.

10. Verdin E. NAD(+) in aging, metabolism, and neurodegeneration. *Science*. 2015;350:1208-13.

11. Choudhary C, Weinert BT, Nishida Y, Verdin E and Mann M. The growing landscape of lysine acetylation links metabolism and cell signalling. *Nature reviews Molecular cell biology*. 2014;15:536-50.

12. Mori V, Amici A, Mazzola F, Di Stefano M, Conforti L, Magni G, Ruggieri S, Raffaelli N and Orsomando G. Metabolic profiling of alternative NAD biosynthetic routes in mouse tissues. *PloS one*. 2014;9:e113939.

13. Yoshino J, Mills KF, Yoon MJ and Imai S. Nicotinamide mononucleotide, a key NAD(+) intermediate, treats the pathophysiology of diet- and age-induced diabetes in mice. *Cell metabolism*. 2011;14:528-36.

14. de Picciotto NE, Gano LB, Johnson LC, Martens CR, Sindler AL, Mills KF, Imai S and Seals DR. Nicotinamide mononucleotide supplementation reverses vascular dysfunction and oxidative stress with aging in mice. *Aging Cell*. 2016;15:522-30.

15. Mills KF, Yoshida S, Stein LR, Grozio A, Kubota S, Sasaki Y, Redpath P, Migaud ME, Apte RS, Uchida K, Yoshino J and Imai SI. Long-Term Administration of Nicotinamide Mononucleotide Mitigates Age-Associated Physiological Decline in Mice. *Cell metabolism*. 2016;24:795-806.

16. Trammell SA, Weidemann BJ, Chadda A, Yorek MS, Holmes A, Coppey LJ, Obrosov A, Kardon RH, Yorek MA and Brenner C. Nicotinamide Riboside Opposes Type 2 Diabetes and Neuropathy in Mice. *Sci Rep*. 2016;6:26933.

17. Trammell SA, Schmidt MS, Weidemann BJ, Redpath P, Jaksch F, Dellinger RW, Li Z, Abel ED, Migaud ME and Brenner C. Nicotinamide riboside is uniquely and orally bioavailable in mice and humans. *Nat Commun*. 2016;7:12948.

18. Zhang H, Ryu D, Wu Y, Gariani K, Wang X, Luan P, D'Amico D, Ropelle ER, Lutolf MP, Aebersold R, Schoonjans K, Menzies KJ and Auwerx J. NAD(+) repletion improves mitochondrial and stem cell function and enhances life span in mice. *Science*. 2016;352:1436-43.

19. Airhart SE, Shireman LM, Risler LJ, Anderson GD, Nagana Gowda GA, Raftery D, Tian R, Shen DD and O'Brien KD. An open-label, non-randomized study of the

pharmacokinetics of the nutritional supplement nicotinamide riboside (NR) and its effects on blood NAD+ levels in healthy volunteers. *PloS one*. 2017;12:e0186459.

20. Bonkowski MS and Sinclair DA. Slowing ageing by design: the rise of NAD(+) and sirtuin-activating compounds. *Nature reviews Molecular cell biology*. 2016;17:679-690.

21. Karamanlidis G, Lee CF, Garcia-Menendez L, Kolwicz SC, Jr., Suthammarak W, Gong G, Sedensky MM, Morgan PG, Wang W and Tian R. Mitochondrial complex I deficiency increases protein acetylation and accelerates heart failure. *Cell metabolism*. 2013;18:239-50.

22. Lee CF, Chavez JD, Garcia-Menendez L, Choi Y, Roe ND, Chiao YA, Edgar JS, Goo YA, Goodlett DR, Bruce JE and Tian R. Normalization of NAD+ Redox Balance as a Therapy for Heart Failure. *Circulation*. 2016;134:883-94.

23. Ido Y, Kilo C and Williamson JR. Cytosolic NADH/NAD+, free radicals, and vascular dysfunction in early diabetes mellitus. *Diabetologia*. 1997;40 Suppl 2:S115-7.

24. Williamson JR, Chang K, Frangos M, Hasan KS, Ido Y, Kawamura T, Nyengaard JR, van den Enden M, Kilo C and Tilton RG. Hyperglycemic pseudohypoxia and diabetic complications. *Diabetes*. 1993;42:801-13.

25. Wu J, Jin Z, Zheng H and Yan LJ. Sources and implications of NADH/NAD(+) redox imbalance in diabetes and its complications. *Diabetes Metab Syndr Obes*. 2016;9:145-53.

26. Berthiaume JM, Hsiung CH, Austin AB, McBrayer SP, Depuydt MM, Chandler MP, Miyagi M and Rosca MG. Methylene blue decreases mitochondrial lysine acetylation in the diabetic heart. *Mol Cell Biochem*. 2017;432:7-24.

27. Vazquez EJ, Berthiaume JM, Kamath V, Achike O, Buchanan E, Montano MM, Chandler MP, Miyagi M and Rosca MG. Mitochondrial complex I defect and increased fatty acid oxidation enhance protein lysine acetylation in the diabetic heart. *Cardiovasc Res*. 2015;107:453-65.

28. Hsu CP, Oka S, Shao D, Hariharan N and Sadoshima J. Nicotinamide phosphoribosyltransferase regulates cell survival through NAD+ synthesis in cardiac myocytes. *Circ Res*. 2009;105:481-91.

29. Carroll PA, Diolaiti D, McFerrin L, Gu H, Djukovic D, Du J, Cheng PF, Anderson S, Ulrich M, Hurley JB, Raftery D, Ayer DE and Eisenman RN. Deregulated Myc requires MondoA/Mlx for metabolic reprogramming and tumorigenesis. *Cancer Cell*. 2015;27:271-85.

30. Chiao YA, Kolwicz SC, Basisty N, Gagnidze A, Zhang J, Gu H, Djukovic D, Beyer RP, Raftery D, MacCoss M, Tian R and Rabinovitch PS. Rapamycin transiently induces mitochondrial remodeling to reprogram energy metabolism in old hearts. *Aging (Albany NY)*. 2016;8:314-27.

31. Gu H, Zhang P, Zhu J and Raftery D. Globally Optimized Targeted Mass Spectrometry: Reliable Metabolomics Analysis with Broad Coverage. *Anal Chem*. 2015;87:12355-62.

32. Wold LE and Ren J. Streptozotocin directly impairs cardiac contractile function in isolated ventricular myocytes via a p38 map kinase-dependent oxidative stress mechanism. *Biochem Biophys Res Commun*. 2004;318:1066-71.

33. Pieper AA, Brat DJ, Krug DK, Watkins CC, Gupta A, Blackshaw S, Verma A, Wang ZQ and Snyder SH. Poly(ADP-ribose) polymerase-deficient mice are protected from streptozotocin-induced diabetes. *Proc Natl Acad Sci U S A*. 1999;96:3059-64.

34. Karunanayake EH, Hearse DJ and Mellows G. Streptozotocin: its excretion and metabolism in the rat. *Diabetologia*. 1976;12:483-8.

35. Russo I and Frangogiannis NG. Diabetes-associated cardiac fibrosis: Cellular effectors, molecular mechanisms and therapeutic opportunities. *Journal of molecular and cellular cardiology*. 2016;90:84-93.

36. Dai DF, Chen T, Szeto H, Nieves-Cintron M, Kutyavin V, Santana LF and Rabinovitch PS. Mitochondrial targeted antioxidant Peptide ameliorates hypertensive cardiomyopathy. *J Am Coll Cardiol*. 2011;58:73-82.

37. Nixon BR, Walton SD, Zhang B, Brundage EA, Little SC, Ziolo MT, Davis JP and Biesiadecki BJ. Combined troponin I Ser-150 and Ser-23/24 phosphorylation sustains thin filament Ca(2+) sensitivity and accelerates deactivation in an acidic environment. *Journal of molecular and cellular cardiology*. 2014;72:177-85.

38. Copeland O, Sadayappan S, Messer AE, Steinen GJ, van der Velden J and Marston SB. Analysis of cardiac myosin binding protein-C phosphorylation in human heart muscle. *Journal of molecular and cellular cardiology*. 2010;49:1003-11.

39. Oliveira SM, Zhang YH, Solis RS, Isackson H, Bellahcene M, Yavari A, Pinter K, Davies JK, Ge Y, Ashrafian H, Walker JW, Carling D, Watkins H, Casadei B and Redwood C. AMP-activated protein kinase phosphorylates cardiac troponin I and alters contractility of murine ventricular myocytes. *Circ Res*. 2012;110:1192-201.

40. Nixon BR, Thawornkaiwong A, Jin J, Brundage EA, Little SC, Davis JP, Solaro RJ and Biesiadecki BJ. AMP-activated protein kinase phosphorylates cardiac troponin I at Ser-150 to increase myofilament calcium sensitivity and blunt PKA-dependent function. *The Journal of biological chemistry*. 2012;287:19136-47.

41. Berthiaume JM, Kurdys JG, Muntean DM and Rosca MG. Mitochondrial NAD(+)/NADH Redox State and Diabetic Cardiomyopathy. *Antioxid Redox Signal*. 2019;30:375-398.

42. Goodman RP, Markhard AL, Shah H, Sharma R, Skinner OS, Clish CB, Deik A, Patgiri A, Hsu YH, Masia R, Noh HL, Suk S, Goldberger O, Hirschhorn JN, Yellen G, Kim JK and Mootha VK. Hepatic NADH reductive stress underlies common variation in metabolic traits. *Nature*. 2020.

43. Hirschey MD, Shimazu T, Jing E, Grueter CA, Collins AM, Aouizerat B, Stancakova A, Goetzman E, Lam MM, Schwer B, Stevens RD, Muehlbauer MJ, Kakar S, Bass NM, Kuusisto J, Laakso M, Alt FW, Newgard CB, Farese RV, Jr., Kahn CR and Verdin E. SIRT3 deficiency and mitochondrial protein hyperacetylation accelerate the development of the metabolic syndrome. *Molecular cell*. 2011;44:177-90.

44. Eto K, Tsubamoto Y, Terauchi Y, Sugiyama T, Kishimoto T, Takahashi N, Yamauchi N, Kubota N, Murayama S, Aizawa T, Akanuma Y, Aizawa S, Kasai H, Yazaki Y and Kadowaki T. Role of NADH shuttle system in glucose-induced activation of mitochondrial metabolism and insulin secretion. *Science*. 1999;283:981-5.

45. Tan C, Tuch BE, Tu J and Brown SA. Role of NADH shuttles in glucose-induced insulin secretion from fetal beta-cells. *Diabetes*. 2002;51:2989-96.

46. Lewandowski ED, O'Donnell J M, Scholz TD, Sorokina N and Buttrick PM. Recruitment of NADH shuttling in pressure-overloaded and hypertrophic rat hearts. *Am J Physiol Cell Physiol*. 2007;292:C1880-6.

47. O'Donnell JM, Kudej RK, LaNoue KF, Vatner SF and Lewandowski ED. Limited transfer of cytosolic NADH into mitochondria at high cardiac workload. *Am J Physiol Heart Circ Physiol*. 2004;286:H2237-42.

48. Mericskay M. Nicotinamide adenine dinucleotide homeostasis and signalling in heart disease: Pathophysiological implications and therapeutic potential. *Arch Cardiovasc Dis*. 2016;109:207-15.

49. Diguet N, Trammell SAJ, Tannous C, Deloux R, Piquereau J, Mougenot N, Gouge A, Gressette M, Manoury B, Blanc J, Breton M, Decaux JF, Lavery GG, Baczko I, Zoll J, Garnier A, Li Z, Brenner C and Mericskay M. Nicotinamide Riboside Preserves Cardiac Function in a Mouse Model of Dilated Cardiomyopathy. *Circulation*. 2018;137:2256-2273.

50. Katsyuba E, Mottis A, Zietak M, De Franco F, van der Velpen V, Gariani K, Ryu D, Cialabrini L, Matilainen O, Liscio P, Giacche N, Stokar-Regenscheit N, Legouis D, de Seigneux S, Ivanisevic J, Raffaelli N, Schoonjans K, Pellicciari R and Auwerx J. De novo NAD(+) synthesis enhances mitochondrial function and improves health. *Nature*. 2018;563:354-359.

NAD^+ Redox Imbalance in the Heart Exacerbates Diabetic Cardiomyopathy

Ying Ann Chiao, PhD[1], Akash Deep Chakraborty, PhD[1,2], Christine M. Light, BS[2], Rong Tian, MD PhD[3], Junichi Sadoshima, MD PhD[4], Xiaojian Shi, PhD[5], Haiwei Gu PhD[5], Chi Fung Lee PhD[2,6*]

[1]Aging and Metabolism Research Program, [2]Cardiovascular Biology Research Program, Oklahoma Medical Research Foundation, Oklahoma City, OK

[3]Mitochondria and Metabolism Center, University of Washington, Seattle, WA

[4]Department of Cell Biology and Molecular Medicine, Rutgers New Jersey Medical School, Newark, NJ

[5]Arizona Metabolomics Laboratory, College of Health Solutions, Arizona State University, Scottsdale, AZ

[6]Department of Physiology, University of Oklahoma Health Sciences Center, Oklahoma City, OK

*** Address correspondence to:**

Chi Fung Lee, PhD
Cardiovascular Biology Research Program, MS 45
Oklahoma Medical Research Foundation
825 NE 13th Street
Oklahoma City, OK 73104, USA
Tel: 405-271-1703
Fax: (405) 271-7417
chifung-lee@omrf.org
Short title: NAD^+ redox balance and diabetic cardiomyopathy

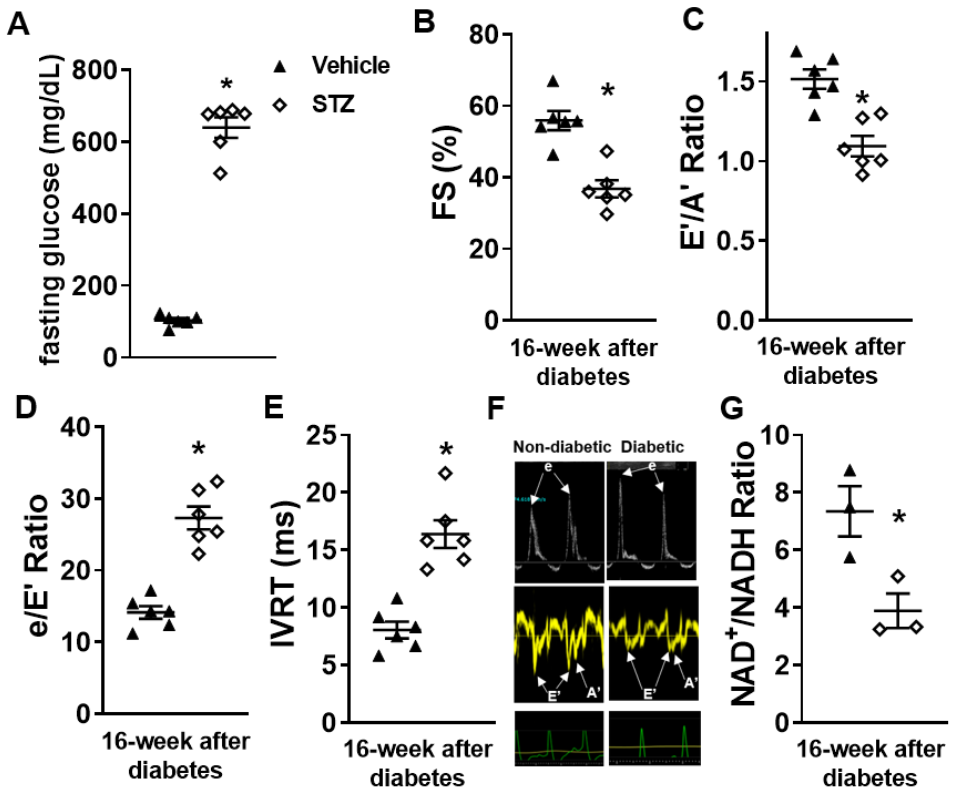

Figure 1. 16-week diabetic stress leads to systolic and diastolic dysfunction and lowered NAD^+/NADH ratio. C57/BL6 wild type (WT) mice were treated with STZ to induce diabetes. Cardiac function was assessed with echocardiography 16 weeks after induction of diabetes. **(A)** Plasma glucose levels were measured 16 weeks after vehicle or STZ treatment. **(B)** Fractional shortening (FS), **(C)** E'/A', **(D)** e/E' ratio, and **(E)** isovolumic relaxation time (IVRT) were measured to evaluate systolic and diastolic functions. N=6. **(F)** Representative pulsed-wave (upper panels) and tissue (middle panels) doppler images and corresponding electrocardiogram (lower panels) images. **(G)** Cardiac NAD^+/NADH ratio were measured. N=3. *: $P<0.05$ to vehicle.

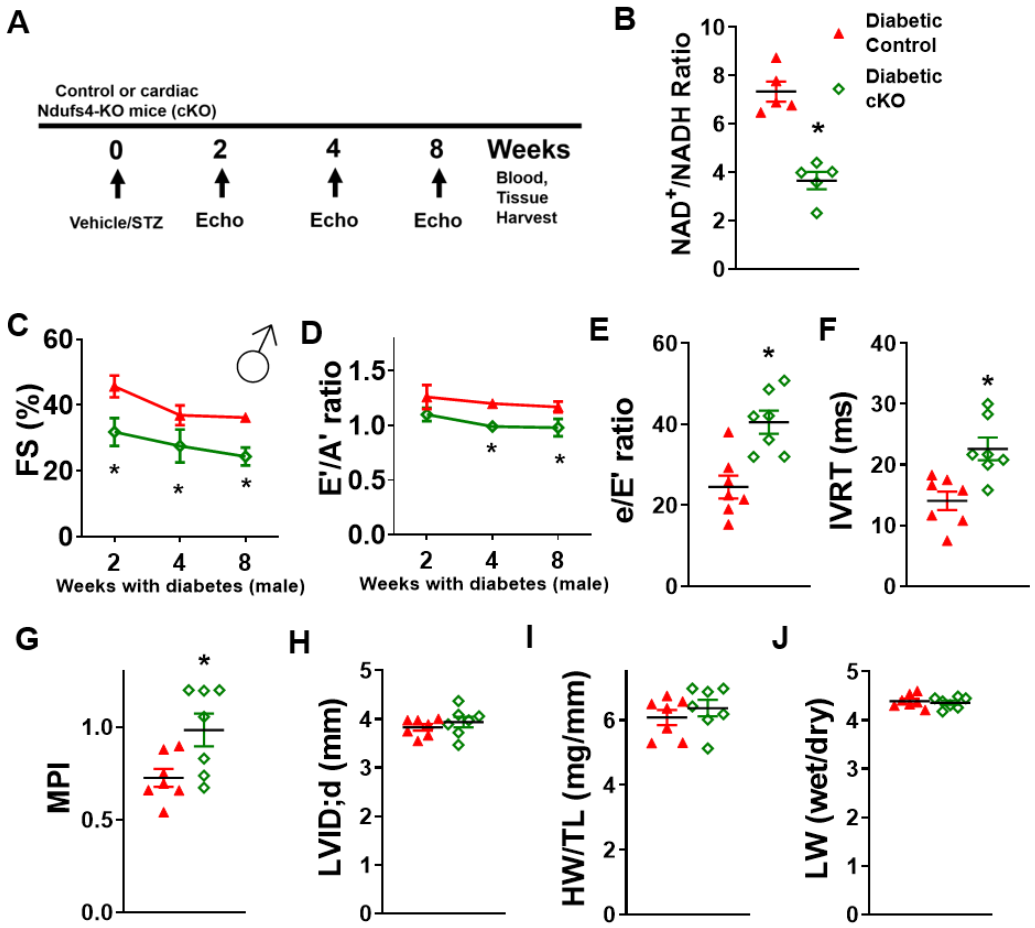

Figure 2. Latent NAD(H) redox imbalance in the heart exacerbates cardiac dysfunctions of diabetic male mice. (A) Experimental plan. Control and cKO male mice were treated with STZ to induce diabetes. Cardiac function was measured at 2, 4, and 8 weeks after induction of diabetes. Blood and tissue samples were collected at the endpoint of the study. **(B)** Cardiac NAD^+/NADH ratio was measured. N=5. Longitudinal changes in **(C)** fractional shortening (FS) and **(D)** E'/A' ratio of diabetic control or cKO male mice were assessed. **(E)** e/E' ratio, **(F)** isovolumic relaxation time (IVRT), **(G)** myocardial performance index (MPI) and **(H)** left ventricular internal dimension at diastole (LVID;d) were measured at 8 weeks after diabetes induction. **(I)** Cardiac hypertrophy (heart weight/tibia length; HW/TL) and **(J)** lung edema of diabetic control or cKO mice (lung wet weight/lung dry weight ratio; LW wet/dry) were determined at 8-week endpoint. N=7. *: $P<0.05$ to diabetic control mice.

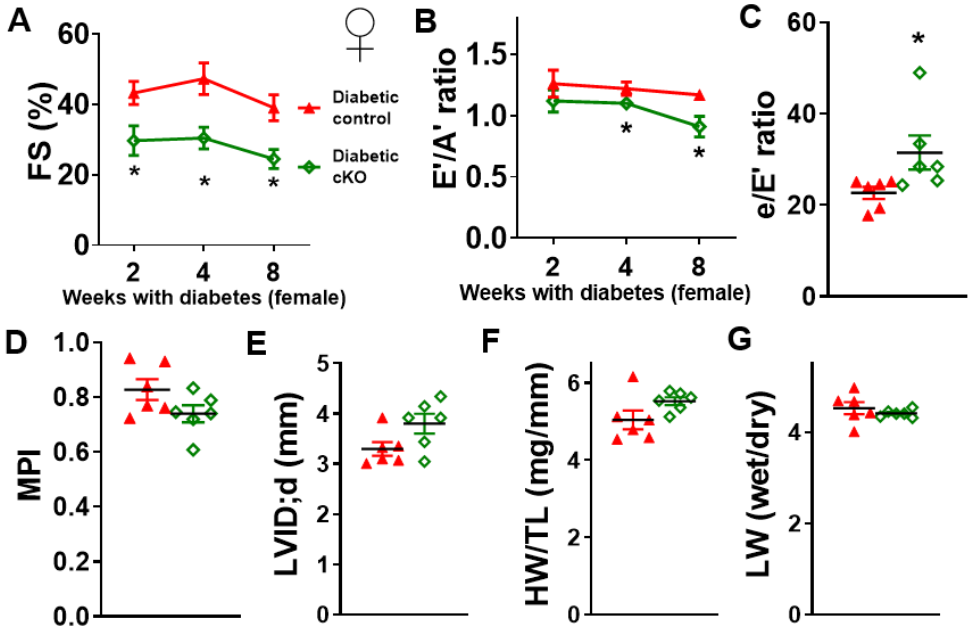

Figure 3. NAD(H) redox imbalance in the heart also exacerbates cardiac dysfunctions of diabetic female mice. Control and cKO female mice were treated with STZ to induce diabetes. Cardiac function was assessed at 2, 4, and 8 weeks after induction of diabetes. **(A)** Longitudinal changes in fractional shortening (FS) and **(B)** E'/A' ratio of diabetic control or cKO female mice were measured. **(C)** e/E' ratio, **(D)** MPI, **(E)** LVID;d, **(F)** HW/TL, and **(G)** LW wet/dry ratio of diabetic control or cKO female mice were determined at 8-week endpoint. N=6. *: P<0.05 to diabetic control mice.

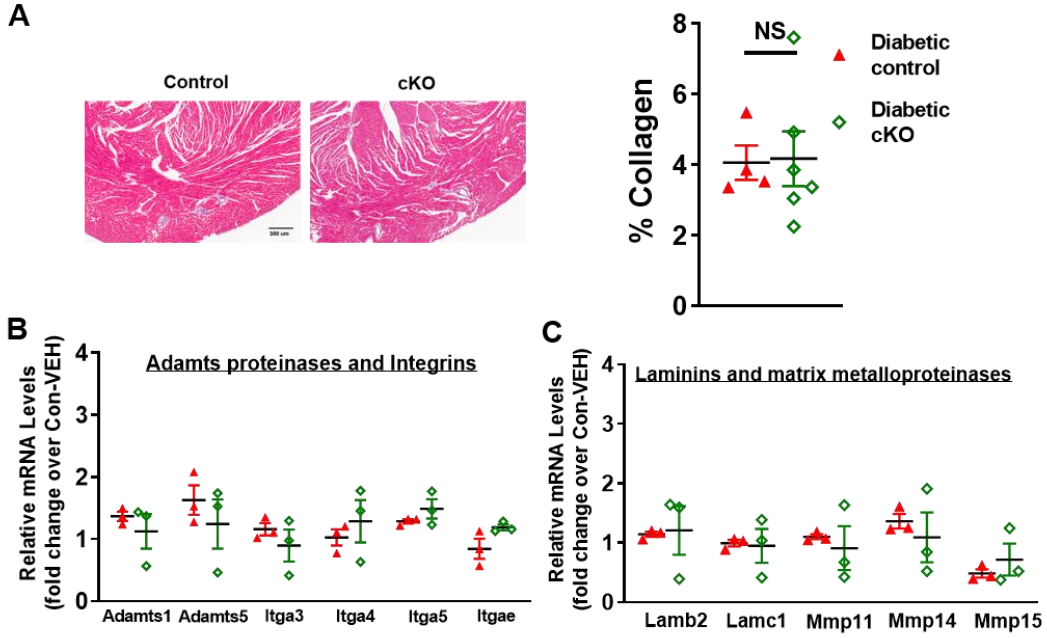

Figure 4. NAD$^+$ redox imbalance exacerbates diabetic cardiomyopathy, independent on tissue fibrosis. (A) Collagen levels of diabetic mouse hearts were quantified by trichrome staining. N=4-6. Transcript expression levels of fibrosis-related genes were quantified by qPCR analyses. **(B)** Adamts proteinases and integrins, and **(C)** laminins and MMPs in diabetic control and diabetic cKO male hearts were measured. N=3. *: P<0.05 to diabetic control mice.

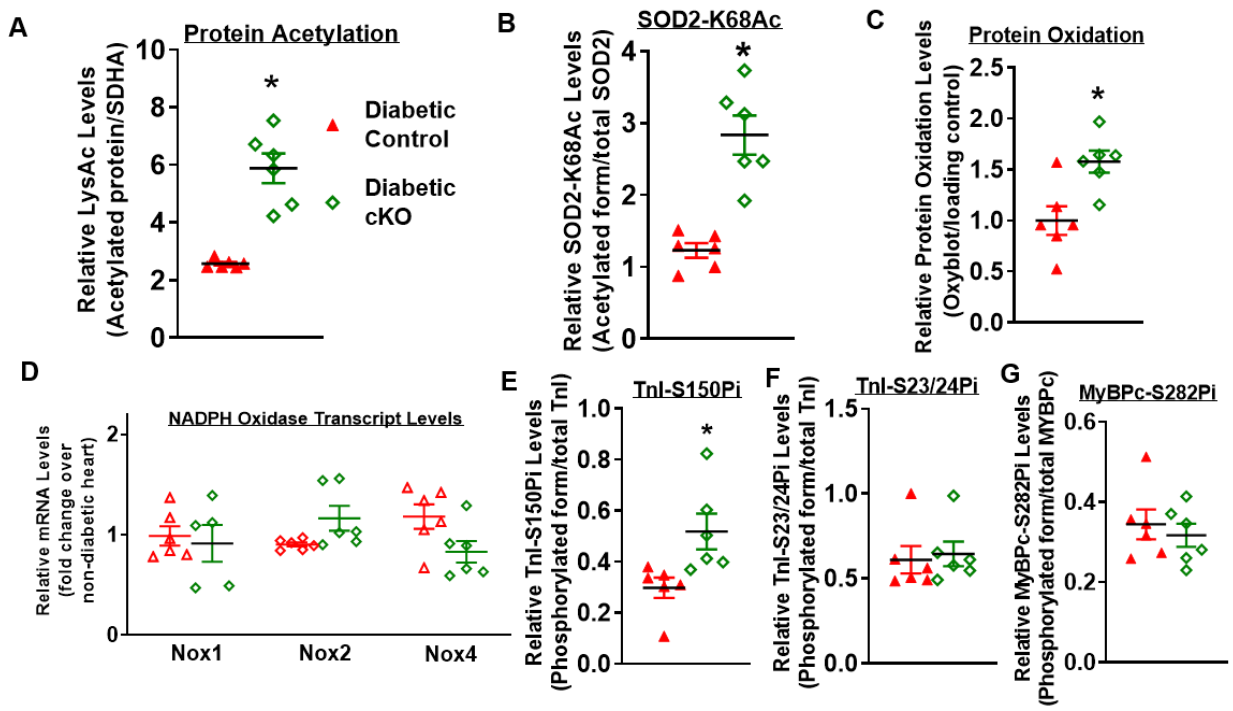

Figure 5. NAD⁺ redox imbalance regulated SOD2 acetylation, protein oxidation and myofilament protein phosphorylation. (A) Global lysine acetylation levels of protein extracts from diabetic control or diabetic cKO hearts were assessed by Western blot. **(B)** Acetylation levels of SOD2 at lysine-68 were assessed by Western blot analysis. **(C)** Protein oxidation levels of diabetic mouse hearts were determined by Oxyblot analysis. **(D)** Relative mRNA levels of pro-oxidant genes (Nox1, Nox2 and Nox4) were measured by qPCR. Phosphorylation levels of myofilament proteins **(E)** TnI at Serine 150 (TnI-S150Pi), **(F)** TnI-S23/24Pi and **(G)** MyBPc at Serine 282 (MyBPc-S282Pi) were measured by Western blot. N=6. *: P<0.05 to diabetic control mice.

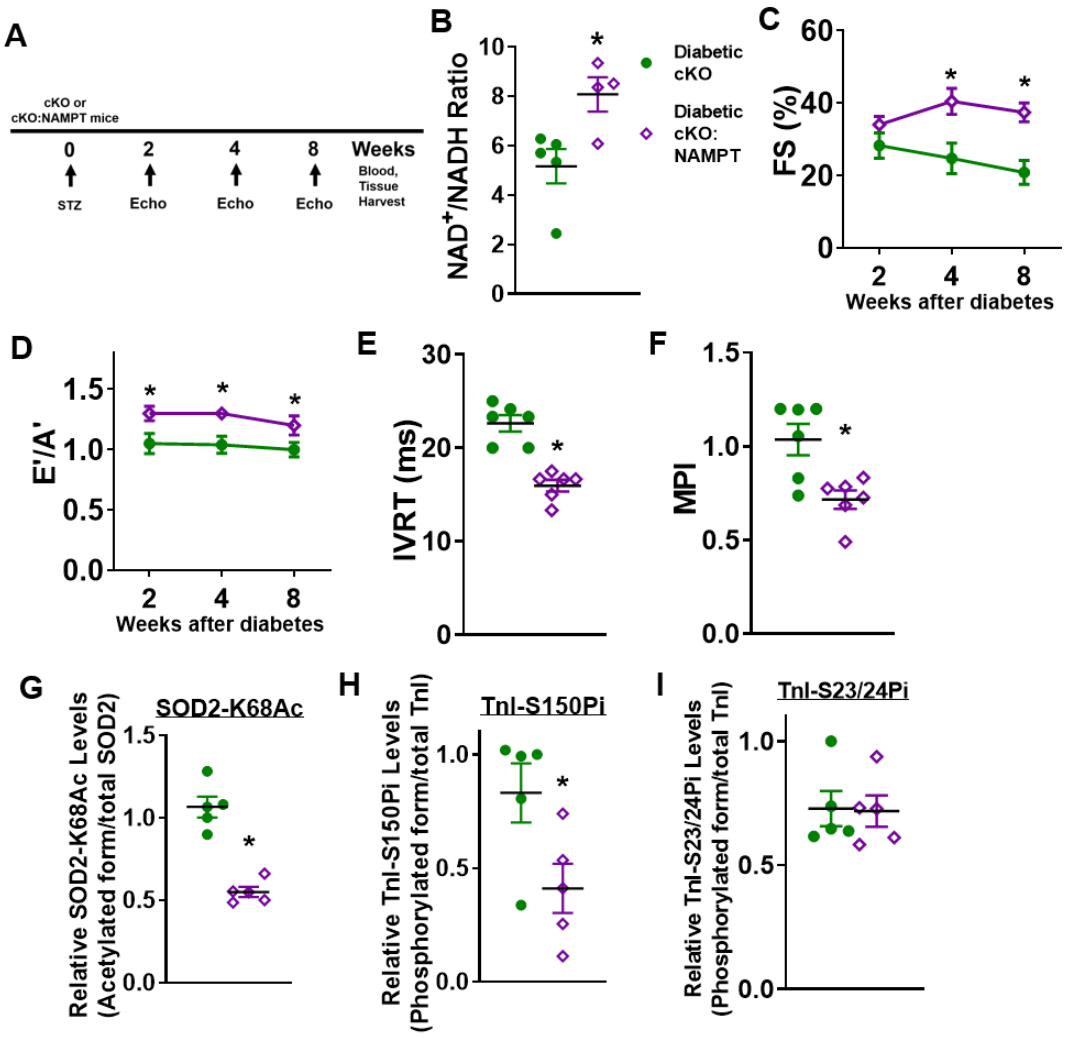

Figure 6. Elevation of cardiac NAD⁺ levels alleviates diabetic cardiomyopathy in cKO mice. (A) Experimental plan. STZ was administered to male cKO and cKO:NAMPT mice to induce diabetes. Cardiac function of cKO and cKO:NAMPT mice was measured at 2, 4, and 8 weeks after induction of diabetes. **(B)** Cardiac NAD^+/NADH ratio were measured. N=4-5. **(C)** FS and **(D)** E'/A' ratio were assessed longitudinally. **(E)** IVRT and **(F)** MPI were measured at 8 weeks after diabetes induction. N=6. Levels of **(G)** SOD2-K68Ac, **(H)** TnI-S150Pi, and **(I)** TnI-S23/24Pi of indicated hearts were measured by Western blots. N=5. *: $P<0.05$ to diabetic cKO mice.

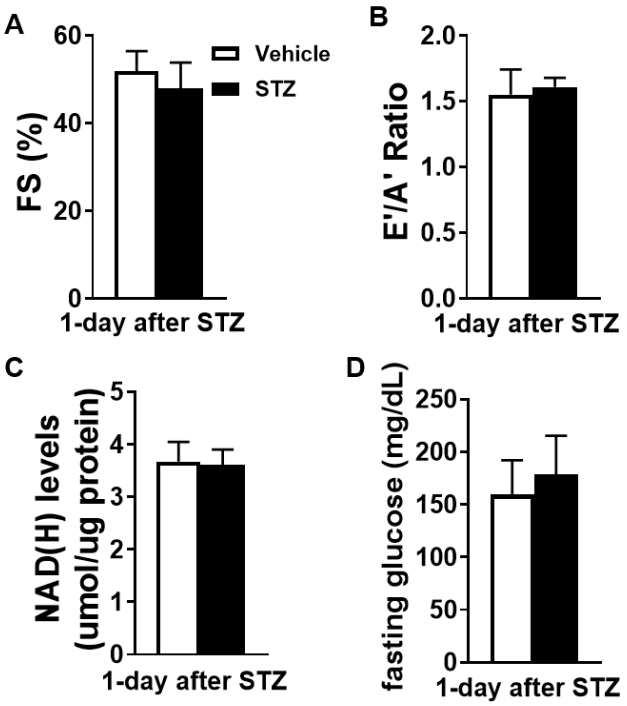

Supplementary Figure 1. STZ treatment does not cause acute changes in contractile function and NAD^+ pool. (A) FS, **(B)** E'/A' ratio and **(C)** NAD(H) pool and **(D)** fasting glucose levels were measured.

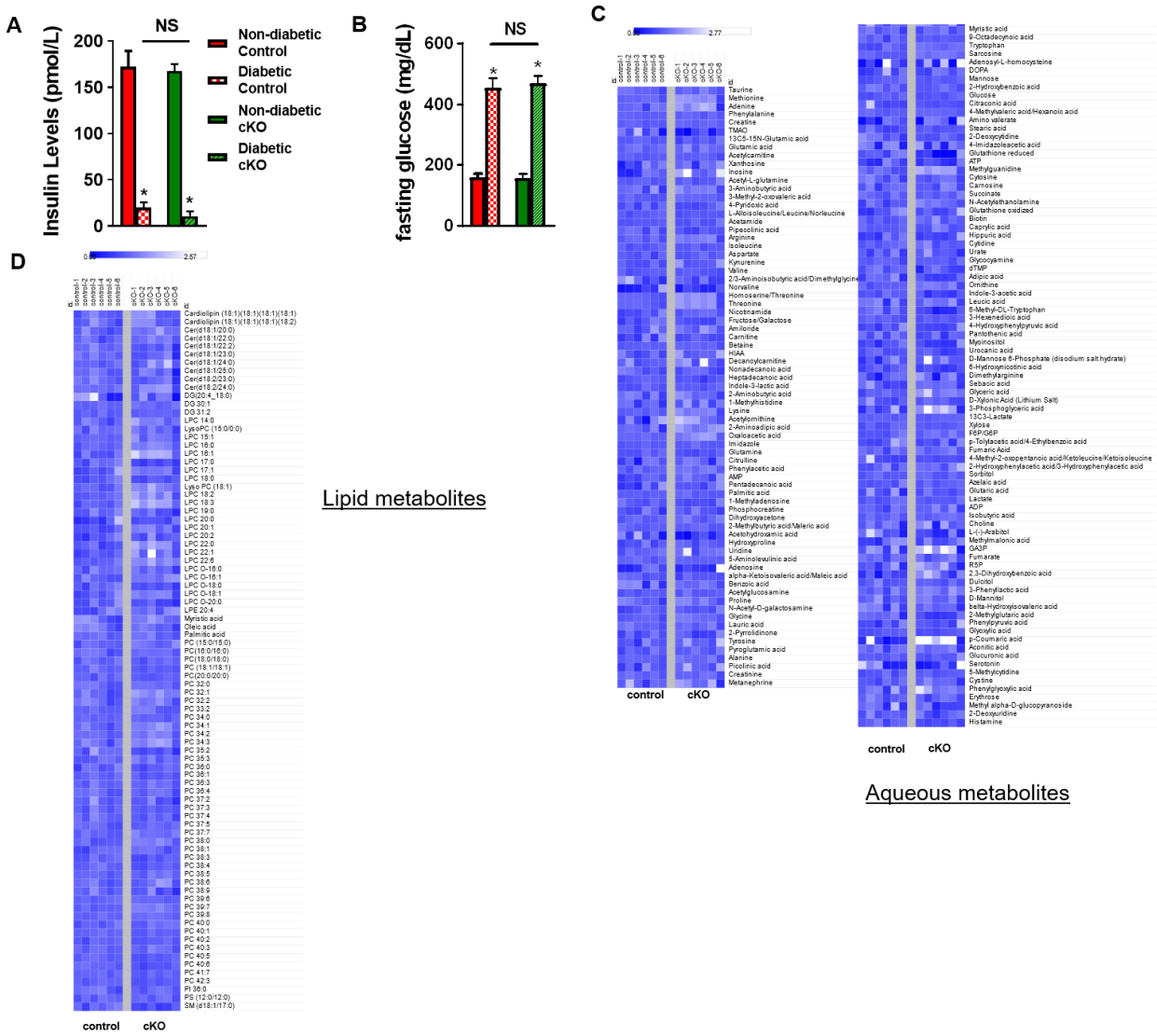

Supplementary Figure 2. (A) Plasma insulin levels and **(B)** fasting glucose levels of male mice with indicated treatment were measured. Heatmaps of **(C)** aqueous and **(D)** lipid metabolite levels in plasma of diabetic control and diabetic cKO mice. Heatmaps were generated using Morpheus. Raw data can be found in supplementary materials. N=6 male mice. *: P<0.05 to corresponding non-diabetic group.

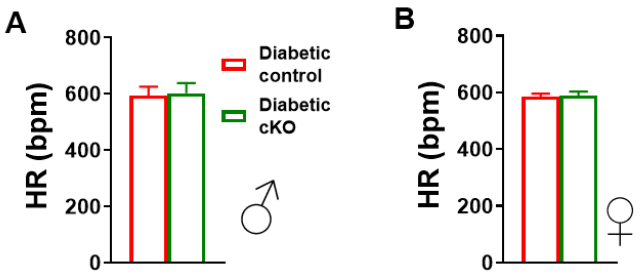

Supplementary Figure 3. Heart rates (HR) of **(A)** male, **(B)** female cohorts of diabetic control and diabetic cKO mice. N=6-7.

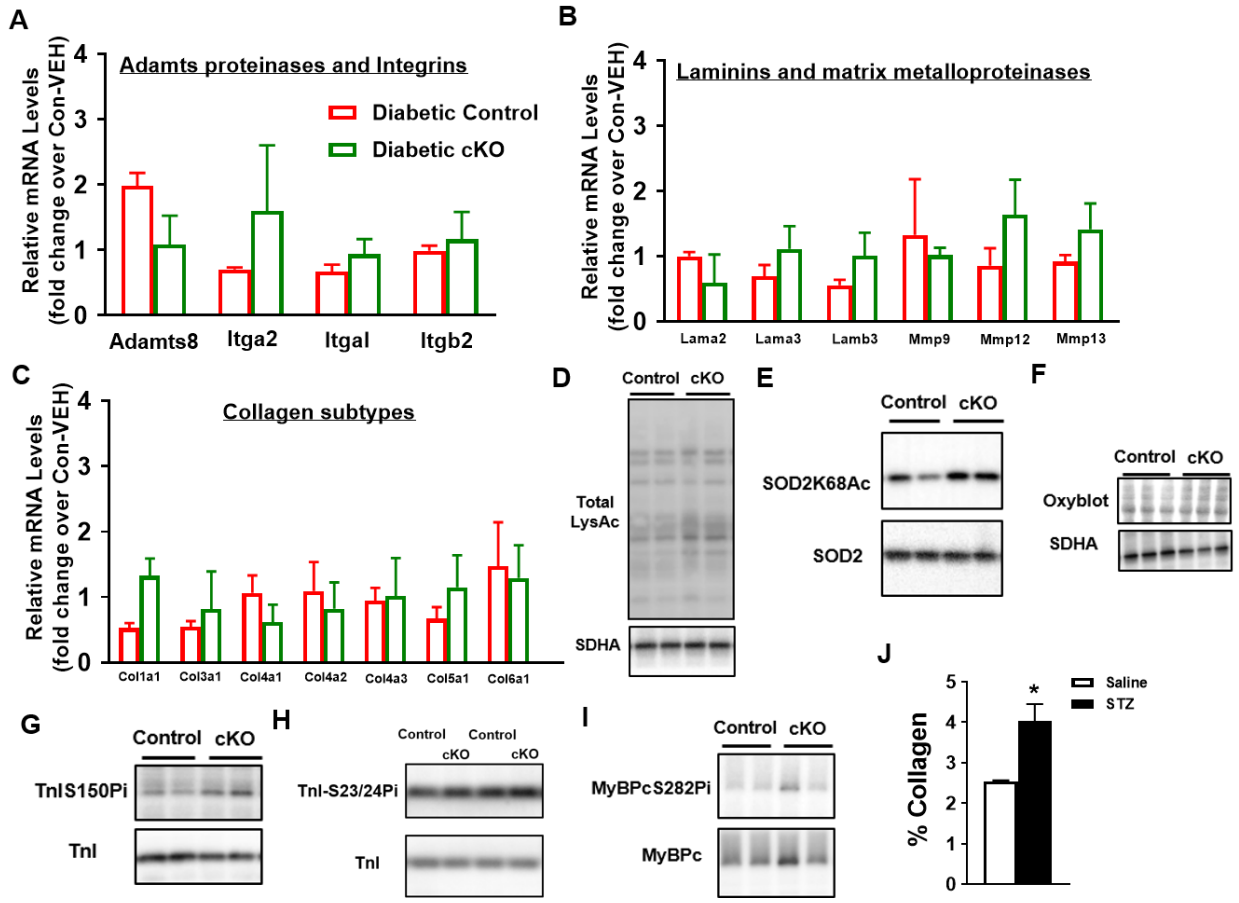

Supplementary Figure 4. Additional gene expression analysis of **(A)** Adamts proteinases and integrins, **(B)** laminins and MMPs, and **(C)** collagen subtypes in diabetic control and diabetic cKO hearts were performed. N=3 male mice. **(D-I)** Representative Western blots for results shown in Figure 5. **(J)** Collagen levels in non-diabetic and STZ-induced diabetic hearts.

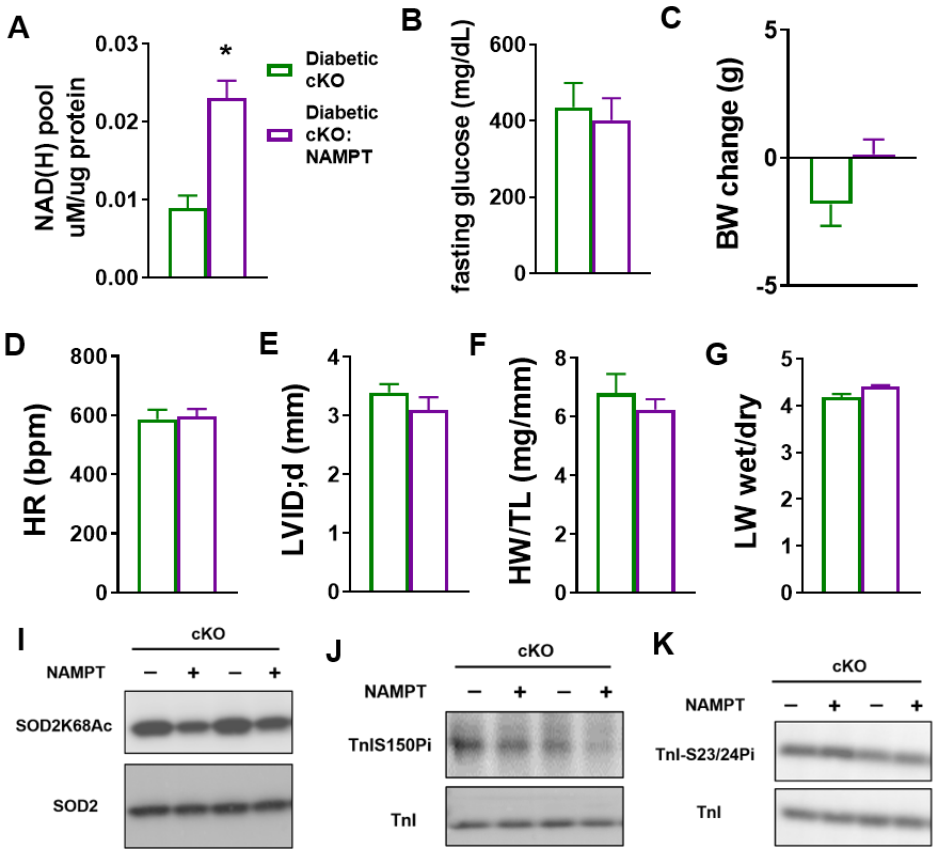

Supplementary Figure 5. (A) NAD^+ pool of diabetic cKO and diabetic cKO:NAMPT mice 8 weeks after STZ treatment were measured. N=5 male mice. **(B)** Fasting glucose levels, **(C)** body weight (BW) change, **(D)** heart rate (HR) at the time acquiring echocardiography data, **(E)** LV dilation, **(F)** hypertrophy and **(G)** lung edema of indicated mice were measured at 8-week endpoint. **(I-K)** Representative Western blots for results shown in Figure 6. *: $P<0.05$ to diabetic cKO mice.